Int. J. Electrochem. Sci., 12 **(2017)** 10534 – 10541, doi: 10.20964/2017.11.08

International Journal of
ELECTROCHEMICAL
SCIENCE
www.electrochemsci.org

Tin Monooxide Monolayer as Promising Anode Materials for Recharge Ion Batteries

Aijian Huang, Xiaoli Sun[*]*, Sha Dong*

School of Physical Electronics, University of Electronic Science and Technology of China, Chengdu, 610054, P.R. China
[*]E-mail: 201511040202@std.uestc.edu.cn

Received: 22 July 2017 / *Accepted:* 28 August 2017 / *Published:* 12 October 2017

Using density functional theory, Li, Na and Mg adsorption and diffusion on a SnO monolayer were investigated. The energetically favored adsorption sites and diffusion paths for Li, Na and Mg were determined. The adsorption energies were in the range of -1.25 ~ -0.94 eV, -0.99 ~ -0.78 eV, and -1.11 ~ -0.66 eV for Li, Na and Mg adsorption with concentrations between x=0.03125-1.0 in M_XSnO (M=Li, Na, or Mg). The volume evolutions were within -4% ~ 8% after Li, Na and Mg adsorption. The smallest energy barriers were 0.31, 0.24 and 0.21 eV for Li, Na and Mg, respectively, diffusing on the SnO monolayer. The SnO monolayer showed strong adsorption stability and low Li, Na and Mg diffusion energy barriers with small volume deformations. Therefore, the SnO monolayer is a promising anode material for rechargeable ion batteries.

Keywords: Monolayer SnO, LIBs, NIBs, MIBs, adsorption energy, diffusion energy

1. INTRODUCTION

Rechargeable ion batteries, such as lithium ion batteries (LIBs), have been widely used as energy conversation and storage devices for portable electronic devices; however, they cannot satisfy the demand of high energy capacity for large-scale energy storage and electric vehicles. Developing a new type of electrode material that can provide a higher power capacity, higher-rate charging/discharging, larger open-circuit voltage and better reversibility of cycling than current commercial battery systems is a main challenge in developing new types of rechargeable ion batteries. Although Si, Ge and Sn anode materials for LIBs possess large capacities of 3579 [1], 1384 [2] and 992 [3] $mA{\cdot}h{\cdot}g^{-1}$, respectively, the huge volume expansion and contraction upon lithium insertion and extraction results in pulverization and degradation of the electrical connection between the electrodes [4], which is a major obstacle for their practical applications in LIBs.

Two-dimensional (2D) materials possess unique physical and chemical properties compared to their bulk counterparts. Their large surface-to-volume ratios can provide many adsorption sites for transporting metal atoms. 2D materials have obtained increasing interest in the fields of energy storage and conversation devices due to their numerous adsorption sites and short diffusion paths. Graphene, a monolayer of graphite, shows a larger energy capacity compared to that of graphite [5, 6]. Transition metal dichalcogenide (TMD) monolayers [7-9], phosphorene [10] and MXenes have been proposed as anode electrode materials for LIBs. A MoS_2 monolayer has a specific density of 1121 $mA{\cdot}h{\cdot}g^{-1}$ [11], which is much higher than that of graphene. Phosphorene as an anode material for LIBs has a specific density of 433 $mA{\cdot}h{\cdot}g^{-1}$ [12]. Other 2D materials, such as V_2O_5 [13], C_3B [14] and Ti_3C_2 [15], have also been studied as potential electrode materials for LIBs.

The limited resources of lithium in nature hinder the further application of LIBs for large-scale energy storage. The development of new battery systems with earth abundant elements is essential to satisfy the increasing demands of energy storage. Sodium shows many similar chemical properties as lithium since it is located below lithium in the periodic table. Magnesium also has chemical similarity to lithium and possesses a similar atomic radius as lithium. The natural abundance of sodium and magnesium make sodium ion batteries (SIBs) and magnesium ion batteries (MIBs) alternatives to LIBs with high energy storage and capacity [16, 17]. It is very urgent to find suitable anode materials for SIBs and MIBs. 2D materials have been investigated for use as anode materials for SIBs and MIBs. Defective graphene can prevent the formation of sodium atom clusters and thus inhibit sodium dendrite growth [18]. Ti_3C_3 MXene has a specific capacity of 351.8 $mA{\cdot}h{\cdot}g^{-1}$ and low diffusion barrier of 0.096 eV for SIBs [19]. Phosphorene, a monolayer of black phosphorus, has a theoretical specific capacity of 865 $mA{\cdot}h{\cdot}g^{-1}$ and low energy barrier of 0.04 eV for NIBs [20]. The sodium diffusion energy barrier on silicene was found to be 0.12 eV [21]. Mg ions showed anisotropic diffusion behavior on phosphorene with a low diffusion energy barrier of 0.08 eV [22].

Tin-based compounds are promising anode materials for LIBs [23, 24]. Tin monooxide (SnO) has a layered structure with weak interlayer interactions [25]. Thus, 2D monolayer SnO can be feasibly synthesized. Nanostructured SnO and composites of carbon nanofibers and SnO have been experimentally synthesized, which exhibited good electrochemical properties [26, 27]. An ideal anode material for rechargeable ion batteries should have a strong ion-binding energy, low-energy ion-diffusion barrier, and low average electrode potential to avoid clustering and achieve fast charging/discharging rates [28]. In this work, we investigated the potential usage of monolayer SnO as anode materials for LIBs, SIBs and MIBs by calculating the Li, Na and Mg adsorption and diffusion energies and the crystal deformations caused by Li, Na and Mg atom adsorption on monolayer SnO using density functional theory (DFT).

2. SIMULATION METHODS

We used the SIEASTA package [29] based on density functional theory for all the calculations. Electronic structure and atomistic geometry calculations were performed using DFT with the generalized gradient approximation (GGA) as parameterized by Perdew, Burke, and Ernzerhof (PBE) [30]. Spin polarization was considered for all the simulations. All the atom positions were optimized

until the magnitudes of forces on them were less than 0.02 eV/Å. The core electrons were represented by norm-conversing Troullier-Martins pseudopotentials. The valence electron wave functions were expanded using a double-ζ basis set plus polarization functional. A real space mesh cut-off of 200 Ry was used for the calculation of the self-consistent Hamiltonian matrix. The directions of the *x*- and *y*-axis were parallel, and the *z*-axis was perpendicular to the SnO monolayer. To avoid the coupling between periodical layers, a vacuum of 30 Å was set along the *z*-axis.

3. RESULTS AND DISCUSSION

3.1 Atomistic structure and band structure of SnO monolayer

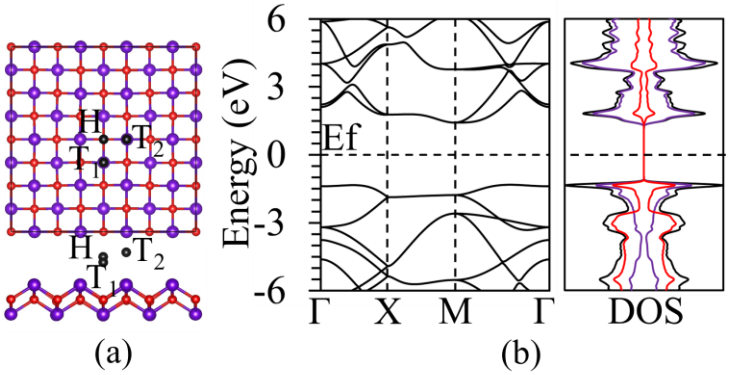

Figure 1. (a) Top and side views of a SnO monolayer. (b) Band structure and DOS of a SnO monolayer.

Bulk SnO possesses a tetragonal structure in the space group *P*4/*nmm*. Along the [001] direction, SnO is displays layered stacking of Sn-O-Sn slabs; the Sn-O-Sn slab consists of an oxygen layer sandwiched between two tin layers. Both O and Sn are four coordinated. The oxygen atoms are the base of a square pyramid with the tin atom located at the apex. The atomistic structure of bulk SnO was first optimized. The calculated lattice constants are: *a*= 3.80 Å and *b*= 3.80 Å, c= 4.84 Å, which agree well with the experimental values of *a*= 3.80 Å, *b*= 3.80 Å and c= 4.836 Å [31, 32] and agrees with previous simulation values of *a*= 3.90 Å, *b*= 3.90 Å and c= 4.95 Å [33]. The lattice constants of a SnO monolayer are *a*= 3.81 Å and *b*= 3.81 Å, which is slightly larger than the corresponding values of the bulk material due to absence of the interactions between layers. As shown in Fig. 1a, a buckled tetragonal structure is formed by each atom bonded to four neighboring atoms. The SnO monolayer is buckled into a zigzag-like line along the *x* and *y* directions. The band structure and density of states (DOS) of the SnO monolayer are shown in Fig. 1b. The SnO monolayer is a semiconductor with a band gap of 2.74 eV.

3.2 Adsorption of Li/Na/Mg on the SnO monolayer

There are three adsorption sites for Li, Na and Mg atoms on the SnO monolayer, which are the H site (the hollow site above the O atom), T1 site (the top site above the bottom Sn atom) and T2 site

(the top site above the upper Sn atom), as shown in Fig. 1a. The adsorption energies of Li, Na and Mg atoms on the SnO monolayer were calculation using equation (1):

$$E_{ads}(\text{Li/Na/Mg}) = (E_{\text{SnO}+n\cdot\text{Li/Na/Mg}} - E_{\text{SnO}} - n\cdot E_{\text{Li/Na/Mg}})/n \quad (1)$$

where $E_{\text{SnO}+n\cdot\text{Li/Na/Mg}}$ and E_{SnO} are the total energies of the supercell with and without adsorption of n number of lithium/sodium/magnesium atoms, respectively. $E_{\text{Li/Na/Mg}}$ is the energy of an isolated Li/Na/Mg atom. A negative adsorption energy represents an exothermic reaction, and a more negative value indicates a more energetically stable adsorption configuration. The energy-favorable adsorption sites for Li, Na and Mg atoms on the SnO monolayer were first studied. The adsorption energies are -0.66, -0.97 and -0.33 eV for Li adsorbed at the H, T1 and T2 sites, respectively. They are -0.55, -0.79 and -0.26 eV for Na adsorbed at the H, T1 and T2 sites, respectively. In addition, they are -0.36, -0.66 and -0.14 eV for Mg adsorbed at adsorbed at the H, T1 and T2 sites, respectively. Li, Na and Mg atoms are all energy favorable to be adsorbed at the T1 site.

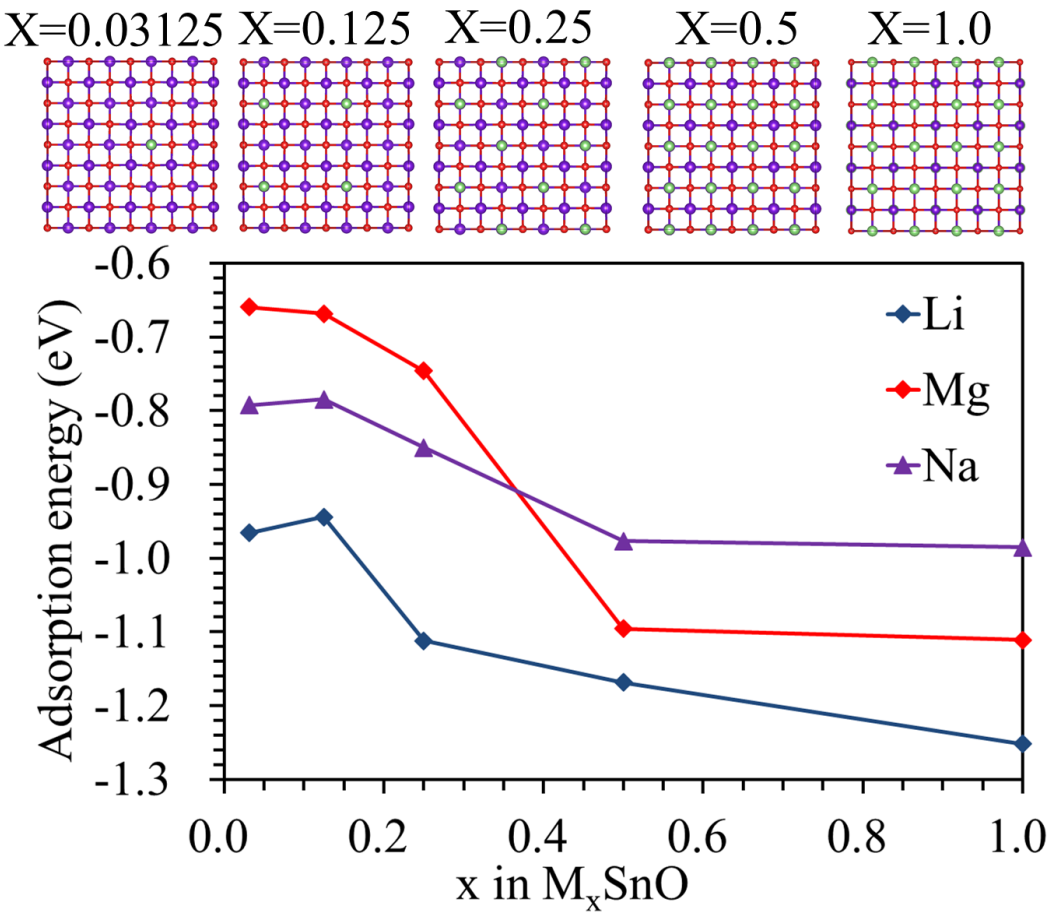

Figure 2. Formation energies as a function of Li/Na/Mg concentrations.

High Li, Na and Mg adsorption concentrations on the SnO monolayer were further studied, and the adsorption energies are shown in Fig. 2, along with the cross-sectional views of the atomic configurations after relaxation. It can be seen from the figure that the adsorption energies decrease

with increasing Li, Na and Mg concentrations. The adsorption energy decreases from -0.94 eV to -1.25 eV as the Li concentration increases from 0.03125 to 1.0 in Li_xSnO.

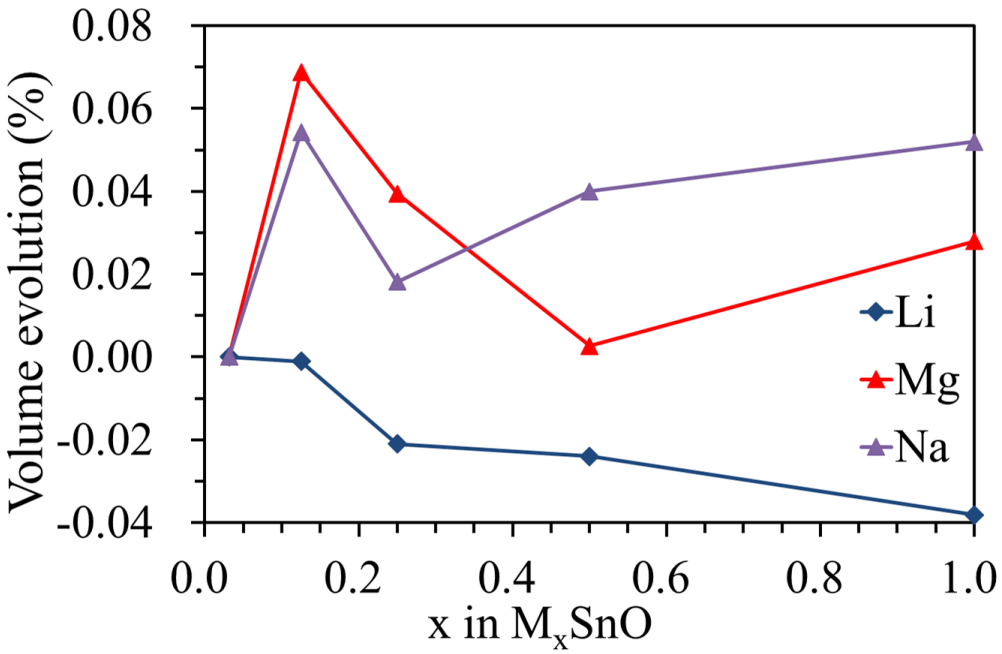

Figure 3. Volume evolution as a function of Li/Na/Mg concentrations.

A good anode material for rechargeable ion batteries should be one with small volume evolution after intercalating ions. The volume changes of the SnO monolayer after Li, Na and Mg adsorption were evaluated by the area changes. The volume evolution is a function of the Li/Na/Mg concentration, as shown in Fig. 3. The volume evolutions by Li/Na/Mg atom adsorption are within the range between -4% and 8%. A small volume change indicates that the SnO monolayer may be used as a safe anode material for rechargeable ion batteries.

3.3 Diffusion energy of Li/Na/Mg on the SnO monolayer

Li/Na/Mg mobility plays a vital role in determining the charging/discharging rate of rechargeable ion batteries, and thus, we further investigated Li/Na/Mg atom diffusion on the SnO monolayer. The diffusion of Li/Na/Mg atoms from one stable T1 site to the nearest one was investigated by considering three possible diffusion pathways in a 4×4 supercell, as shown in Fig. 4a. Diffusion path 1 is from the T1 site to the nearest T1 site by passing the H site, path 2 is from the T1 site to a near T1 site by passing the T2 site, and path 3 is the diffusion from the H site to a near H site by passing the T2 site. The energy profiles for Li, Na and Mg diffusion along the three paths are shown in Fig. 4b, 4c and 4d, respectively. The Li diffusion energy barriers are 0.31, 0.64 and 0.33 eV for Li along path 1, path 2 and path 3, respectively. Li can diffuse on the entire SnO monolayer almost homogeneously through path 1 and path 3. The Na diffusion energy barriers are 0.24, 0.53 and 0.29 eV along path 1, path 2 and path 3, respectively. In addition, the Mg diffusion energy barriers are 0.30, 0.52 and 0.21 eV along path 1, path 2 and path 3, respectively. Na diffuses easily along path 1,

whereas Mg diffuses easily along path 3. Na and Mg show anisotropic diffusion behavior on the SnO monolayer.

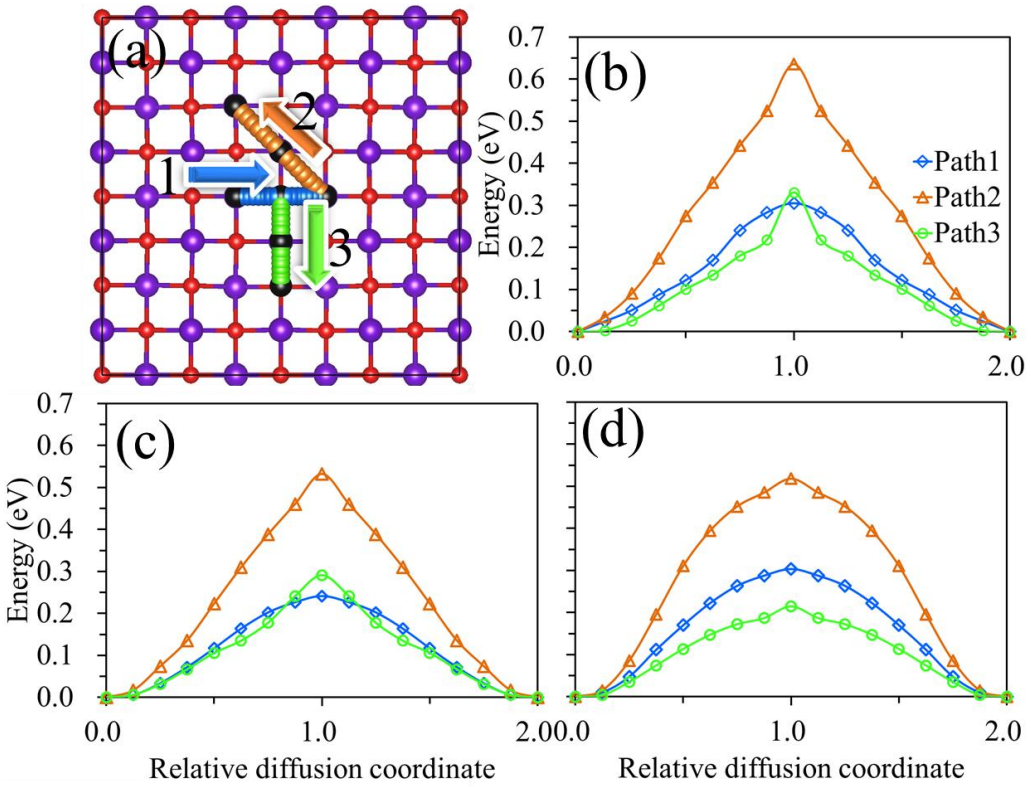

Figure 4. (a) Three diffusion paths and the energy barrier profiles of (b) Li, (c) Na, (d)Mg diffusion on the SnO monolayer.

Li/Mg/Na atoms have relatively low diffusion energy barriers on the SnO monolayer, which are comparable to other two-dimensional materials. For example, the low Li diffusion barrier (0.31 eV) is comparable to those on graphene (0.26 eV) [34], a MoS_2 monolayer (0.21 eV) [7], a MoS_2 bilayer (0.32 eV) [35] and a BP monolayer (0.36 eV) [36], which indicates that the SnO monolayer can exhibit high charging/discharging rates as an anode for LIBs. Similarly, although the low Na diffusion barrier (0.21 eV) is larger than that on a MoS_2 monolayer (0.11 eV) [37], the Na diffusion barrier is comparable to those on graphene (0.19 eV) [18] and a BP monolayer (0.22) [36], which demonstrates that the SnO monolayer may be used as an anode material for NIBs. In addition, for Mg ion batteries, the low diffusion energy barrier (0.21 eV) is larger than that on monolayer Nb_2C (0.10 eV) [38] and smaller than those on layered $Na_{0.66}[Li_{0.22}Ti_{0.78}]O_2$ (0.4 eV) [39] and monolayer Cr_2CO_2 (0.50 eV) [40], which corresponds to a reasonable value for using the SnO monolayer as an anode materials for MIBs.

4. CONCLUSION

In conclusion, Li, Na and Mg adsorption and diffusion on a SnO monolayer were investigated using first principles calculations. The energetically favored adsorption sites and diffusion paths for Li,

Na and Mg were studied. The adsorption energies were in the range of -1.25 ~ -0.94 eV, -0.99 ~ -0.78 eV, and -1.11 ~ -0.66 eV for Li, Na and Mg adsorption with concentrations between x=0.03125-1.0 in M_XSnO (M=Li, Na, or Mg). The volume evolution was within -4% ~ 8% after Li, Na and Mg adsorption, which indicates that SnO can be used as a safe anode material for rechargeable ion batteries. The smallest diffusion energy barriers were 0.31, 0.24 and 0.21 eV for Li, Na and Mg, respectively, diffusing on the SnO monolayer. The SnO monolayer had strong adsorption stability and low diffusion energy barriers for Li, Na and Mg with small volume deformations. Therefore, the SnO monolayer is a promising anode material for rechargeable ion batteries.

ACKNOWLEDGEMENT
This work was financially supported by the National Natural Science Foundation of China (11474047) and the Fundamental Research Funds for the Central Universities (ZYGX2016J202). This work was carried out at the National Supercomputer Center in Tianjin, and the calculations were performed on TianHe-1(A).

References

1. U. Kasavajjula, C. Wang and A. J. Appleby, *J. Power Sources*, 163 (2007) 1003.
2. C. Zhang, Z. Lin, Z. Yang, D. Xiao, P. Hu, H. Xu, Y. Duan, S. Pang, L. Gu and G. Cui, *Chem. Mater.*, 27 (2015) 2189.
3. H. Li, X. Huang and L. Chen, *Solid State Ionics*, 123 (1999) 189.
4. G. Kim, S. Jeong, J.-H. Shin, J. Cho and H. Lee, *ACS Nano*, 8 (2014) 1907.
5. G. Wang, X. Shen, J. Yao and J. Park, *Carbon*, 47 (2009) 2049.
6. D. Wang, R. Kou, D. Choi, Z. Yang, Z. Nie, J. Li, L. V. Saraf, D. Hu, J. Zhang, G. L. Graff, J. Liu, M. A. Pope and I. A. Aksay, *ACS Nano*, 4 (2010) 1587.
7. X. Sun, Z. Wang and Y. Q. Fu, *Sci. Rep.*, 5 (2015) 18712.
8. X. Sun, Z. Wang, Z. Li and Y. Q. Fu, *Sci. Rep.*, 6 (2016) 26666.
9. W. Shi, Z. Wang, Z. Li and Y. Q. Fu, *Mater. Chem. Phys.*, 183 (2016) 392.
10. W. Li, Y. Yang, G. Zhang and Y. W. Zhang, *Nano Lett*, 15 (2015) 1691.
11. J. Xiao, D. Choi, L. Cosimbescu, P. Koech, J. Liu and J. P. Lemmon, *Chem. Mater.*, 22 (2010) 4522.
12. S. Zhao, W. Kang and J. Xue, *J. Mater. Chem. A.*, 2 (2014) 19046.
13. Z. Wang, Q. Su and H. Deng, *Phys. Chem. Chem. Phys.*, 15 (2013) 8705.
14. Y. Y. Liu, V. I. Artyukhov, M. J. Liu, A. R. Harutyunyan and B. I. Yakobson, *J. Phys.Chem. Lett.*, 4 (2013) 1737.
15. Q. Tang, Z. Zhou and P. Shen, *J. Am. Chem. Soc.*, 134 (2012) 16909.
16. N. Yabuuchi, M. Kajiyama, J. Iwatate, H. Nishikawa, S. Hitomi, R. Okuyama, R. Usui, Y. Yamada and S. Komaba, *Nat. Commun.*, 11 (2012) 512.
17. H. D. Yoo, I. Shterenberg, Y. Gofer, G. Gershinsky, N. Pour and D. Aurbach, *Energ. Environ. Sci.*, 6 (2013) 2265.
18. X. Sun, Z. Wang and Y. Q. Fu, *Carbon*, 116 (2017) 415.
19. D. Er, J. Li, M. Naguib, Y. Gogotsi and V. B. Shenoy, *ACS Appl Mater Interfaces*, 6 (2014) 11173.
20. V. V. Kulish, O. I. Malyi, C. Persson and P. Wu, *Phys. Chem. Chem. Phys.*, 17 (2015) 13921.
21. V. V. Kulish, O. I. Malyi, M. F. Ng, Z. Chen, S. Manzhos and P. Wu, *Phys. Chem. Chem. Phys.*, 16 (2014) 4260.
22. W. Jin, Z. Wang and Y. Q. Fu, *J. Mater. Sci.*, 51 (2016) 7355.

23. M. N. Obrovac, L. Christensen, D. B. Le and J. R. Dahn, *J. Electrochem. Soc.*, 154 (2007) A849.
24. Y. Idota, Y. M. Matsufuji, T. Miyasaka, and A. T. Kubota, *Science*, 276 (1997) 1395.
25. J. P. Allen, D. O. Scanlon, S. C. Parker and G. W. Watson, *J. Phys.Chem. C*, 115 (2011) 19916.
26. W. Yue, S. Yang, Y. Ren and X. Yang, *Electrochim. Acta*, 92 (2013) 412.
27. K. Sakaushi, Y. Oaki, H. Uchiyama, E. Hosono, H. Zhou and H. Imai, *Small*, 6 (2010) 776.
28. Q. Yao, C. Huang, Y. Yuan, Y. Liu, S. Liu, K. Deng and E. Kan, *J. Phys.Chem. C*, 119 (2015) 6923.
29. J. M. Soler, E. Artacho, J. D. Gale, Alberto Garcıa, J. Junquera, P. Ordejon and D. Sanchez-Portal, *J. Phys. Condens. Matte.*, 14 (2002) 2745.
30. J. Perdew, K. Burke and M. Ernzerhof, *Phys. Rev. Lett.*, 77 (1996) 3865.
31. H. Giefers, F. Porsch and G. Wortmann, *Phys. B: Condensed Matt*, 373 (2006) 76.
32. H. Giefers, S. Koval, G. Wortmann, W. Sturhahn, E. E. Alp and M. Y. Hu, *Phys. Rev. B.*, 74 (2006) 094303.
33. M. A. Ali, A. K. M. A. Islam, N. Jahan and S. Karimunnesa, *Int. J. Mod Phys. B.*, 30 (2016) 1650228.
34. D. H. Wu, Y. F. Li and Z. Zhou, *Theor. Chem. ACC.*, 130 (2011) 209.
35. Y. Li, D. Wu, Z. Zhou, C. R. Cabrera and Z. Chen, *J. Phys. Chem. Lett.*, 3 (2012) 2221.
36. H. R. Jiang, W. Shyy, M. Liu, L. Wei, M. C. Wu and T. S. Zhao, *J. Mater. Chem. A*, 5 (2017) 672.
37. J. Su, Y. Pei, Z. Yang and X. Wang, *RSC Adv.*, 4 (2014) 43183.
38. J. Hu, B. Xu, C. Ouyang, Y. Zhang and S. A. Yang, *RSC Adv.*, 6 (2016) 27467.
39. Y. S. Wang, X. Q. Yu, S. Y. Xu, J. M. Bai, R. J. Xiao, Y. S. Hu, H. Li, X. Q. Yang, L. Q. Chen and X. J. Huang, *Nat. Commun.*, 4 (2013) 2365.
40. F. Li, C. R. Cabrera, J. Wang and Z. Chen, *RSC Adv.*, 6 (2016) 81591.